Quantized Conductance in a CVD-Grown Nanoribbon with Hidden Rashba Effect

Jianfei Xiao,[1,2,*] Yiwen Ma,[1,2,*] Congwei Tan,[3,*,†] Kui Zhao,[1,4] Yunteng Shi,[1,2] Bingbing Tong,[1,5] Peiling Li,[1,5] Ziwei Dou,[1] Xiaohui Song,[1,5] Guangtong Liu,[1,5] Jie Shen,[1] Zhaozheng Lyu,[1,5] Li Lu,[1,2,5,‡] Hailin Peng,[3,§] and Fanming Qu[1,2,5,‖]

[1]*Beijing National Laboratory for Condensed Matter Physics, Institute of Physics, Chinese Academy of Sciences, Beijing 100190, China*

[2]*University of Chinese Academy of Sciences, Beijing 100049, China*

[3]*Center for Nanochemistry, Beijing National Laboratory for Molecular Sciences, College of Chemistry and Molecular Engineering, Peking University, Beijing 100871, China*

[4]*Beijing Key Laboratory of Fault-Tolerant Quantum Computing, Beijing Academy of Quantum Information Sciences, Beijing 100193, China*

[5]*Hefei National Laboratory, Hefei 230088, China*

(Received 16 June 2025; accepted 23 December 2025; published 27 January 2026)

Quantized conductance in quasi-one-dimensional systems not only provides a hallmark of ballistic transport, but also serves as a gateway for exploring quantum phenomena. Recently, a unique hidden Rashba effect, which arises from the compensation of opposite spin polarizations of a Rashba bilayer in inversion symmetric crystals with dipole fields, such as bismuth oxyselenide (Bi_2O_2Se), has attracted tremendous attention. However, investigating this effect utilizing conductance quantization remains challenging. Here we report the conductance quantization observed in a chemical vapor deposition (CVD)-grown high-mobility Bi_2O_2Se nanoribbon, where quantized conductance plateaus up to $44 \times 2e^2/h$ (e is the elementary charge, h is the Planck's constant, and the factor 2 results from spin degeneracy) are achieved at zero magnetic field. Because of the hidden Rashba effect, the quantized conductance remains in multiples of $2e^2/h$ without Zeeman splitting even under magnetic field up to 12 T. Moreover, within a specific range of magnetic field, the plateau sequence follows the Pascal triangle series, namely, $(1, 3, 6, 10, 15\ldots) \times 2e^2/h$, reflecting the interplay of size quantization in the two transverse directions. These observations are well captured by an effective hidden Rashba bilayer model. Our results demonstrate Bi_2O_2Se as a compelling platform for spintronics and the investigation of emergent phenomena.

DOI: 10.1103/vtjc-znrb

Introduction—The observation of quantized conductance, in units of $2e^2/h$ where e is the elementary charge, h is the Planck's constant, and the factor 2 originates from the spin degeneracy, serves as a hallmark of ballistic transport in quasi-one-dimensional (quasi-1D) systems. Moreover, conductance quantization also plays an important role in investigating quantum phenomena, such as correlation effects [1], and the Kronig-Penney model [2]. Quantized conductance was first achieved in quantum point contacts (QPCs) defined on III-V two-dimensional electron gases (2DEGs) [3–6], leveraging their high mobility and gate tunability, followed by metallic break junctions [7,8] and other two-dimensional (2D) systems [9–13]. Subsequently, advances in material quality enabled the observation of quantized conductance in ultraclean individual 1D systems [14–17], e.g., nanowires, nanoribbons, and nanotubes. However, the reported quantized plateaus are mostly limited to indices below 10 (namely, quantized conductance plateau $G \leq 10 \times 2e^2/h$).

Recently, a novel 2D semiconductor Bi_2O_2Se has garnered significant attention [18–22] owing to its outstanding electronic properties, including a moderate band gap, small effective mass, ultrahigh carrier mobility, and strong spin-orbit coupling (SOC), together with responsiveness to diverse external stimuli. Crucially, its excellent air stability and native oxide high-κ dielectric (Bi_2SeO_5) [23,24] further enhance its potential for high-performance 2D electronic devices, including 2D-FinFET [18] and gate-all-around FET (GAAFET) [25]. Notably, previous investigations have primarily focused on 2D Bi_2O_2Se. Herein, we choose quasi-1D Bi_2O_2Se nanoribbon as the platform to investigate ballistic transport approaching high quantized indices, particularly involving hidden Rashba effect and Pascal triangle series, as detailed in the following.

First, due to the large Fermi velocity [26], suppressed electron back-scattering [22], and the self-modulation

*These authors contributed equally to this work.
†Contact author: tancw-cnc@pku.edu.cn
‡Contact author: lilu@iphy.ac.cn
§Contact author: hlpeng@pku.edu.cn
‖Contact author: fanmingqu@iphy.ac.cn

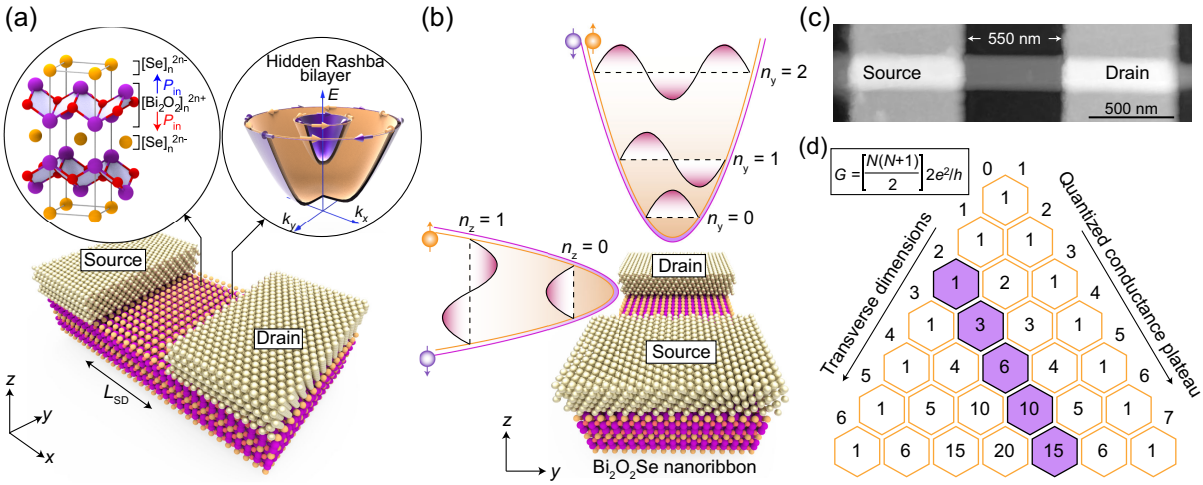

FIG. 1. (a) Schematic of the Bi_2O_2Se nanoribbon device. The left inset illustrates the layered crystal structure. The right inset depicts the hidden Rashba effect arising from the unique Rashba bilayer structure. The bands in different colors represent different spin textures, while the arrows stand for the spin orientations. (b) Illustration of the confining potential, identical for the two spin textures. For clarity, the two confining potentials for two degenerate spins are slightly separated. (c) AFM image of the device. (d) Pascal triangle of the quantized conductance, described by $G = [N(N+1)/2]2e^2/h$ for the highlighted diagonal with the transverse dimension of 2.

doping [27], Bi_2O_2Se gains remarkably high mobility [21]. Interestingly, the mechanism of self-modulation doping stems from the spatial separation between the conductive $[Bi_2O_2]_n^{2n+}$ layers and the defect-rich $[Se]_n^{2n-}$ layers, which effectively minimizes impurity scattering. This exceptional high-mobility has facilitated the demonstration of quantum Hall effect (QHE) [28,29]. Second, the combination of the inversion symmetry and the intrinsic dipole field in Bi_2O_2Se gives rise to a unique hidden Rashba effect. This effect provides efficient electrical tunability for spin FET [30,31], and has been probed by angular resolved photoemission spectroscopy and photocurrent in, e.g., WSe_2 [32,33], BSCCO(2212) [34], ZrSiTe [35], and GdSbTe [36], while more evidence from electrical transport experiment remains scarce. Furthermore, the hidden Rashba effect with spin-layer locking exhibits a distinct spin texture that maintains spin degeneracy even under high magnetic fields [28], facilitating quasi-1D ballistic transport as a probe for this phenomenon. Third, size quantization in a ballistic system along two transverse directions under the harmonic-oscillator-type parabolic potentials induces a complex evolution of conductance quantization, which could follow a characteristic pattern of the Pascal triangle series [1,37]. Considering the electron-electron interaction [38], Bi_2O_2Se serves as a promising platform for investigating correlation effects [1].

In this Letter, we report the conductance quantization behavior, combined with the hidden Rashba effect, in high-quality chemical vapor deposition (CVD)-grown Bi_2O_2Se nanoribbons. Quantized conductance plateaus up to $44 \times 2e^2/h$ are observed, the highest in individual 1D systems. In particular, owing to the hidden Rashba effect resulted from the unique Rashba bilayer structure, the conductance quantization remains at multiples of $2e^2/h$—rather than Zeeman-splitting-induced e^2/h—even under magnetic fields up to 12 T. Furthermore, within a range of magnetic field, the sequence of quantized conductance plateaus follows the Pascal series. These experimental results are well reproduced by theoretical calculations based on an effective hidden Rashba bilayer model.

Results—Bi_2O_2Se nanoribbons are grown by CVD method [39,40], and the two-terminal devices are fabricated by standard electron-beam lithography techniques (see Supplemental Material Sec. A [41]). Figure 1(a) depicts a schematic of the device, where a Bi_2O_2Se nanoribbon is contacted by the source and drain, with a channel length $L_{SD} \approx 550$ nm. Notably, Bi_2O_2Se features an inversion-symmetric crystal structure, where tetragonal $[Bi_2O_2]_n^{2n+}$ and $[Se]_n^{2n-}$ layers are staggered and stacked along the c axis [68]. As schematically depicted in the left inset of Fig. 1(a), the two Bi monolayers in the $[Bi_2O_2]_n^{2n+}$ layers form a peculiar hidden Rashba bilayer due to opposite interlayer polarizations [28] (labeled by P_{in} in different colors). The alternating dipole fields break the local inversion symmetry of the monolayers, giving rise to opposite strong Rashba effects with compensated spin textures, which results in the hidden Rashba effect [69]. In this scenario, as illustrated in the right inset of Fig. 1(a), each band is 2-fold degenerate, with an expected extremely small effective g factor, indicating suppressed Zeeman splitting under high magnetic fields.

Figure 1(b) depicts the confining potential of spin-degenerate electrons, which come from different monolayers of the hidden Rashba bilayer. A perpendicular magnetic field B along the z direction modulates the electrostatic confining potential in the y direction [70], thereby effectively tuning the size quantization in the nanoribbon. The lowest several sublevels denoted by $n_i = 0, 1, 2, \ldots$ (where $i = y, z$) are the quantized states in y and z directions, respectively. Figure 1(c) presents the atomic force microscopy (AFM)

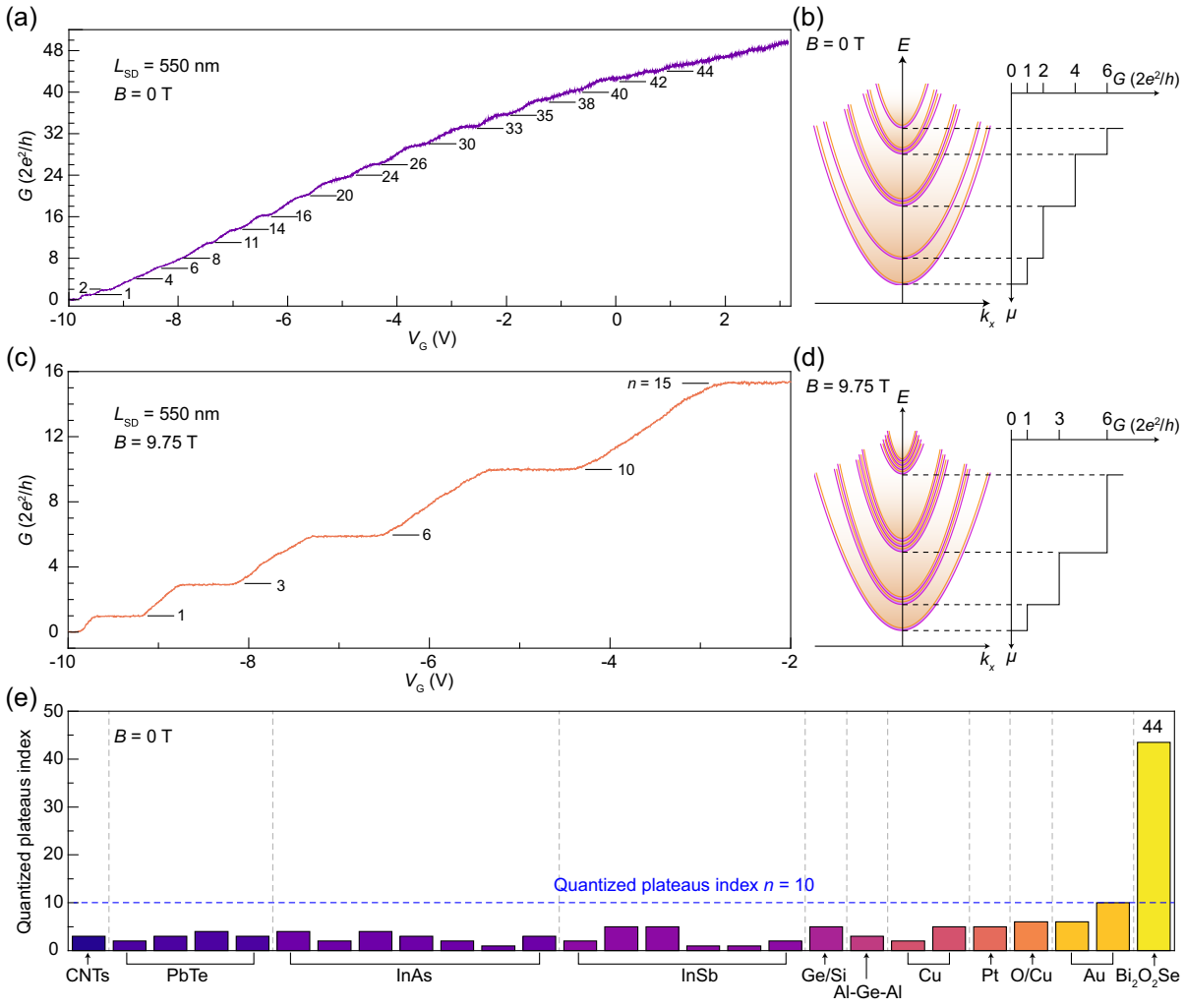

FIG. 2. (a) Quantized conductance (G), expressed in units of $2e^2/h$ as a function of gate voltage V_G at $B = 0$ T and $T = 1.5$ K. (c) Quantized conductance at $B = 9.75$ T, which exhibits a novel degeneracy of quantized conductance steps following the Pascal triangle sequence. (b),(d) Fermi level alignments corresponding to the quantized conductance observed in (a) and (c), respectively. (e) Survey of quantized plateau index among individual 1D materials [16,17,42–63].

image of the device, with a thickness of 50 nm. As shown in Fig. 1(d), as a result of the size quantization in the two transverse directions of the nanoribbon, the quantized conductance under a range of magnetic fields follows the characteristic sequence $G = [N(N+1)/2]2e^2/h$ (where $N = 1, 2, 3, \ldots$), corresponding to the purple diagonal in the Pascal triangle. The hidden Rashba effect, responsible for the spin degenerate bands, leads to the persistence of quantized conductance being multiples of $2e^2/h$.

To demonstrate the quantized conductance behavior of our Bi_2O_2Se nanoribbon device, we performed low-temperature ($T = 1.5$ K) transport measurements under perpendicular magnetic fields applied along the z direction [Fig. 1(b)]. A series resistance of 350 Ω, determined from the deviation of the first plateau at $B = 12$ T from the expected conductance of $2e^2/h$, was subtracted from all measured resistance data. In addition, all the conductance traces were measured at zero dc bias voltage, unless otherwise stated.

At $B = 0$ T [Fig. 2(a)], a series of quantized conductance plateaus with indices reaching 44 (in units of $2e^2/h$) are observed as the gate voltage V_G is varied. It is noteworthy that the index of 44 not only far exceeds the previous maximum of 10 in individual 1D systems [see Fig. 2(e) and Supplemental Material Sec. B [41]], but also ranks among the highest values reported for QPCs defined on 2D systems [3,9,71–73]. Moreover, the authenticity of the high-index plateaus is supported by temperature-dependent data, reference devices, and further analysis (Supplemental Material Secs. C–E [41]). From the fitting of the V_G -dependent conductance (G) curve in Fig. 2(a), we extract the field-effect mobility $\mu \sim 1.11 \times 10^4$ cm^2 V^{-1} s^{-1} (Supplemental Material Sec. F [41]). The absence of certain plateaus (namely, $\nu = 3, 5, 7, 9, 10, \ldots$) in Fig. 2(a) can be generally attributed to the degenerate subbands as schematically represented by the Fermi level alignment conditions in Fig. 2(b). The degeneracies arise

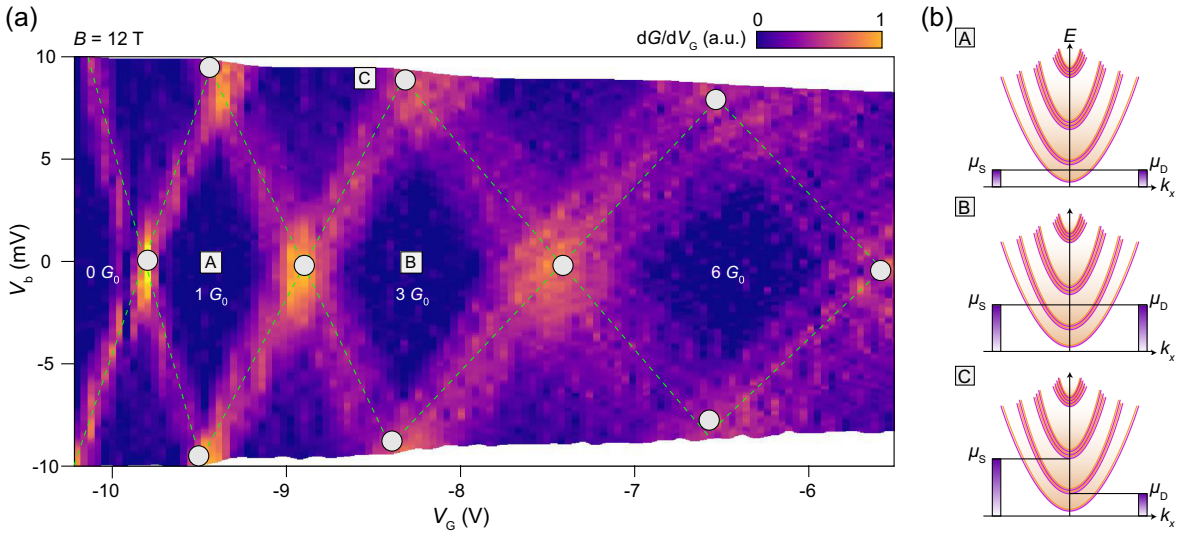

FIG. 3. (a) Normalized transconductance (dG/dV_G) map as a function of V_G and V_b, where $G_0 = 2e^2/h$. (b) Fermi level alignment conditions, labeled by A, B, and C in (a).

from the specific confining potentials in the y and z directions, which are influenced by device geometry, interface, disorder, etc. In other words, conductance plateau transitions occur when the Fermi level aligns with the bottoms of subbands, whose degeneracy is governed by the confining potentials. It is crucial to point out that each parabolic band contributes a quantized conductance of e^2/h. When B is increased to 9.75 T, the conductance trace as a function of V_G [Fig. 2(c)] exhibits two remarkable characteristics. First, the quantized conductance remains in units of $2e^2/h$, indicating the suppression of Zeeman splitting because of the hidden Rashba effect. Second, an unconventional quantized plateau series following the Pascal triangle, i.e., $1, 3, 6, 10, 15 \times (2e^2/h)$, is observed, implying a unique band degeneracy, schematically depicted in Fig. 2(d), which will be discussed later.

We then applied a dc bias voltage V_b to investigate the spectroscopy of the conductance quantization. Figure 3 presents the spectroscopy measurement at $B = 12$ T, revealing a series of quantized conductance of $1, 3, 6\times (2e^2/h)$, which is also in good conformity with the highlighted diagonal of the Pascal triangle in Fig. 1(d). For clarity, the normalized transconductance dG/dV_G is plotted as a function of V_G and V_b in Fig. 3(a), where the transitions between quantized conductance plateaus are represented by the bright regions. Furthermore, diamond-shaped regions outlined by dashed lines connecting the circles correspond to the conductance plateaus quantized in multiples of $2e^2/h$.

In Fig. 3(b) the Fermi level alignments noted by A, B, and C, where μ_s and μ_D denote the chemical potentials of the source and drain, respectively, illustrate the corresponding conditions in Fig. 3(a). Conductance traces measured at different magnetic fields (Supplemental Material Sec. G [41]) consistently maintain the quantization in units of $2e^2/h$. Moreover, transconductance spectroscopy under different magnetic fields (Supplemental Material Sec. H [41]) reveals that certain quantized plateaus (e.g., $2G_0, 3G_0, 4G_0, \ldots$) gradually emerge and/or disappear as B increases, indicating an unusual magnetic field dependence of the subband evolution.

To explore the evolution of quantized conductance with magnetic field (B), we plot conductance traces as a function of V_G in Fig. 4(a) for fields ranging from 0 to 12 T in steps of 0.25 T. The indices of the quantized conductance plateaus are labeled (demonstration of individual conductance curves, along with alternative versions of the conductance map are provided in Supplemental Material Sec. I [41]). Notably, half-integer plateaus [including 0.5 and $1.5 \times (2e^2/h)$] do not develop under magnetic fields up to 12 T [Fig. 4(a)], reflecting the suppression of Zeeman splitting due to the hidden Rashba effect, as can also be seen in Fig. 2(c) and the spectroscopy of Fig. 3(a).

To further analyze the evolution of the quantized conductance plateaus, Figs. 4(b) and 4(c) present renormalized transconductance ($dG/d\mu$) and conductance maps as a function of B and chemical potential μ, respectively (the conversion from V_G to μ, i.e., the gate lever arm, is explained in Supplemental Material Sec. J [41]). Particularly, in Fig. 4(b), quantized conductance plateaus appear as dark purple regions, some of which are labeled with their indices, whereas bright boundaries delineating these regions stand for the evolution of subbands induced by size quantization along the two transverse directions. These subband evolutions are traced in Fig. 4(b), and then they can be categorized and grouped by their slopes with respect to μ under high magnetic fields, as shown by the solid lines with different colors in Fig. 4(c) and detailed in Supplemental Material Sec. K [41]. By tracking the origin of each subband to low magnetic fields, we find that they originate from energy quantization along both y and z

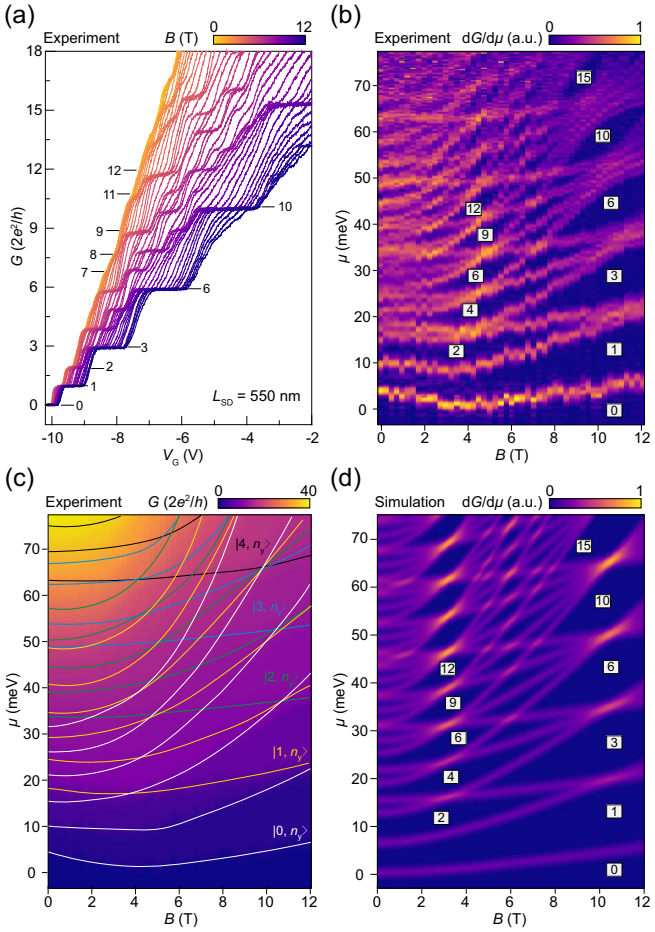

FIG. 4. (a) Quantized conductance evolution under different magnetic fields plotted as a function of V_G. Renormalized transconductance, $dG/d\mu$, (b) and conductance, G, (c) maps plotted against μ and B, respectively. (d) Simulation of $dG/d\mu$ based on the effective model [Eq. (2)], demonstrating consistency with (b) and (c), considering a broadening of 0.7 meV. The numbers label the quantized conductance indices, while $|n_z, n_y\rangle$ denotes the subbands.

directions: subbands of different colors correspond to quantization due to the finite thickness along the z direction, whereas those of the same color stem from the constrained width along the y direction. Accordingly, subbands are labeled in the form $|n_z, n_y\rangle$ in Fig. 4(c) and Fig. S14 [41], where n_y and n_z denote the quantum numbers associated with size quantization in y and z directions, respectively.

To describe the quantized conductance behavior, we establish an effective hidden Rashba bilayer model that includes confining potentials along both the y direction, which is modulated by magnetic field, and z direction. In fact, under zero magnetic field, the level spacings between subbands quantized along the y direction—represented by the same color in Fig. 4(c) corresponding to the same n_z but varying n_y—are nearly identical. Similarly, subbands resulting from quantization along the z direction, namely, those represented by different colors with fixed n_y but varying n_z, exhibit equal spacings as well. This naturally suggests that the confining potentials in both y and z directions can both be well approximated by a harmonic oscillator potential, whose quantized energy levels possess equidistant spacing described by $E_\xi = (\xi + 1/2)\hbar\omega$ (where ω is the eigenfrequency, ξ is the level index). Thus, the effective Hamiltonian for the system can be expressed as $H = [(\boldsymbol{p} + e\boldsymbol{A})^2/2m'] + \frac{1}{2}g'\mu_B B\sigma_z + \frac{1}{2}m'\omega_y^2 y^2 + \frac{1}{2}m'\omega_z^2 z^2$, where m' and g' are the renormalized effective mass and effective g-factor obtained from *ab initio* calculations based on a hidden Rashba bilayer model involving multi-bilayers, μ_B denotes the Bohr magneton, σ is the Pauli matrix, $\boldsymbol{A} = A_x\boldsymbol{e}_x = -By\boldsymbol{e}_x$ represents the vector potential, $\omega_{y,z}$ denote the eigenfrequencies of the confining potentials in y and z directions, respectively.

Such an effective model describes the subbands with the following form:

$$E(n_y, n_z; B) = \hbar\Omega\left(n_y + \frac{1}{2}\right) + \hbar\omega_z\left(n_z + \frac{1}{2}\right) \pm \frac{1}{2}g'\mu_B B, \tag{1}$$

where $\Omega = \sqrt{\omega_c^2 + \omega_y^2}$, and $\omega_c = eB/m'$ is the cyclotron frequency. Due to the unavoidable effects caused by finite temperature and measurement noise, energy broadening occurs, resulting in the smearing of the density of states, which may hinder the differentiation of Zeeman splitting at magnetic fields up to 12 T. Here, we assume a Gaussian broadening $W(\mu; \varepsilon_0, \Gamma) = (1/\sqrt{2\pi}\Gamma)e^{-(\mu-\varepsilon_0)^2/(2\Gamma^2)}$ with $\Gamma = 0.7$ meV determined from the Gaussian fitting of the measured spectroscopy (Supplemental Material Sec. L [41]).

To obtain m' and g' on the basis of the hidden Rashba effect together with interlayer coupling, we performed an *ab initio* calculation for a 40-unit-cell-thick Bi_2O_2Se nanoribbon, consistent with the thickness of 50 nm (Supplemental Material Sec. M [41]). Herein, the Rashba SOC strength α alternates in sign between successive $[Bi_2O_2]_n^{2n+}$ layers along the z axis, analogous to a Su-Schrieffer-Heeger chain [74]. Orbital effects induced by the magnetic field are implemented via the Peierls substitution, $\boldsymbol{p} \to \boldsymbol{p} + e\boldsymbol{A}$. Subsequently, through an exact unitary transformation, the Hamiltonian can be expressed in the Landau levels basis [75] as

$$\begin{aligned} H_{nn'}^{ll'} = {} & \hbar\frac{eB}{m^*}\left(n + \frac{1}{2}\right)\delta_{nn'}\delta_{ll'}\sigma_0 \\ & + \frac{1}{2}g_e\mu_B B\delta_{nn'}\delta_{ll'}\sigma_z - t\delta_{nn'}\delta_{l,l'\pm1}\sigma_0 \\ & + (-1)^l\frac{-i\alpha}{\sqrt{2}\ell_B}\delta_{ll'}\left(\sqrt{n+1}\delta_{n,n'-1}\sigma_+ - \sqrt{n}\delta_{n,n'+1}\sigma_-\right), \end{aligned} \tag{2}$$

where n is the quantum number of Landau levels, l is the layer index, $\sigma_\pm = \sigma_x \pm i\sigma_y$, $\ell_B = \sqrt{\hbar/eB}$ is the magnetic

length, $g_e = 2$ is the bare Landé g-factor, and t represents the interlayer coupling.

By taking $\alpha = 1.45$ eV · Å [28], we find that when $m^* = 0.08m_e$ and correspondingly $t = 0.32$ eV, the simulation agrees well with the experimental data, yielding renormalized $m' = 0.084m_e$ and $g' = 0.78$. Notably, the suppression of g' to 0.78 is induced by the hidden Rashba effect and interlayer hybridization (Supplemental Material Sec. M [41]). Specifically, spin-conserved interlayer coupling hybridizes subbands with opposite spin textures originating from monolayers with $+\alpha$ and $-\alpha$, namely, the hidden Rashba effect. This effect further competes with the bare Zeeman effect, leading to the suppressed $g' = 0.78$ which is smaller than the upper bound $g_{\mathrm{sup}} = 1.18$ estimated from the experimental energy resolution (Supplemental Material Sec. M [41]). Therefore, Zeeman splitting remains undetectable even at 12 T. As shown in Fig. 4(d), the simulation exhibits good agreement with the experimental observations, confirming the conductance quantization as a reliable method for investigating this effect.

Finally, to better understand the Pascal-like quantized conductance plateaus observed at high magnetic fields, we begin with Eq. (1), which demonstrates that the subband energy can be simplified as a linear combination $\eta n_y + \zeta n_z$, where η and ζ represent the coefficients. The fact that the magnetic field modulates the confining potential in y direction, effectively results in a corresponding adjustment of η. The index of a conductance plateau at a specific chemical potential μ_0 corresponds to the number of subbands intersecting the Fermi level, which is determined by counting the natural-number solutions to the inequality $\eta n_y + \zeta n_z \leq \mu_0$. For instance, in Fig. 4(b), $\eta = \zeta$ is satisfied around 10 T, and the amount of natural-number solutions (subbands below the Fermi level) to $n_y + n_z \leq \mathrm{const}$ defines the conductance plateau indices, which follow a series corresponding to Pascal triangle with the transverse dimension of 2. As a result, $G = [\mathrm{N}(\mathrm{N}+1)/2]2e^2/h$, i.e., $G = 1, 3, 6, 10, 15 \times (2e^2/h)$, as observed experimentally. Moreover, it is necessary to clarify that the missing plateaus at zero magnetic field are due to the accidental degeneracies arising from the given device conditions, while the Pascal sequence at $B \sim 10$ T results from the interplay of quantization in the two transverse directions originating from the two harmonic oscillators.

Conclusions—In conclusion, we have demonstrated ballistic transport in CVD-grown Bi_2O_2Se nanoribbons. We observed a record-high quantized conductance plateau index of 44 at zero magnetic field, the maintenance of multiples of $2e^2/h$ even under magnetic fields up to 12 T because of the unique hidden Rashba effect, and the Pascal triangle series. By means of an effective hidden Rashba bilayer model, we demonstrated spectra that agreed well with our experiment.

The observation of ultrahigh quantized conductance plateaus provides a clear signature of ballistic transport, where disorder represents a significant barrier to the practical implementation of quasi-1D materials in applications such as Majorana zero modes [76]. Furthermore, the spin-layer locking, manifested by the peculiar hidden Rashba effect, positions Bi_2O_2Se as a promising candidate for investigating unique properties [69], including piezoelectricity and second-harmonic generation, which were previously thought to only exist in inversion-asymmetric systems. Moreover, its exceptional electrical tunability and high mobility reinforce its potential for spintronic applications, such as electrically controlled spin FET [30,31]. Beyond its relevance to applications, Bi_2O_2Se also offers a fertile ground for exploring emergent phenomena, including the spin Hall effect and nonlinear physics, and could be a compelling platform to investigate correlation effects [1] considering the electron-electron interaction [38].

Acknowledgments—This work was supported by the National Key Research and Development Program of China (No. 2025YFE0217600, No. 2022YFA1403400, and No. 2025YFA1411400); by the National Natural Science Foundation of China (No. 92065203, No. 92365207, No. 22572004, No. T2588301, and No. 22432001); by the Strategic Priority Research Program of Chinese Academy of Sciences (No. XDB33000000); by the Synergetic Extreme Condition User Facility sponsored by the National Development and Reform Commission; by the Innovation Program for Quantum Science and Technology (No. 2021ZD0302600 and No. 2021ZD0301800); and by the New Cornerstone Science Foundation through the New Cornerstone Investigator Program and the XPLORER PRIZE.

Data availability—The data that support the findings of this article are openly available [77].

[1] M. Briggeman *et al.*, Pascal conductance series in ballistic one-dimensional $LaAlO_3/SrTiO_3$ channels, Science **367**, 769 (2020).

[2] M. Briggeman *et al.*, One-dimensional Kronig–Penney superlattices at the $LaAlO_3/SrTiO_3$ interface, Nat. Phys. **17**, 782 (2021).

[3] B. J. van Wees, H. van Houten, C. W. J. Beenakker, J. G. Williamson, L. P. Kouwenhoven, D. van der Marel, and C. T. Foxon, Quantized conductance of point contacts in a two-dimensional electron gas, Phys. Rev. Lett. **60**, 848 (1988).

[4] D. A. Wharam, T. J. Thornton, R. Newbury, M. Pepper, H. Ahmed, J. E. F. Frost, D. G. Hasko, D. C. Peacock, D. A. Ritchie, and G. A. C. Jones, One-dimensional transport and the quantisation of the ballistic resistance, J. Phys. C **21**, L209 (1988).

[5] R. Crook, J. Prance, K. J. Thomas, S. J. Chorley, I. Farrer, D. A. Ritchie, M. Pepper, and C. G. Smith, Conductance

quantization at a half-integer plateau in a symmetric GaAs quantum wire, Science **312**, 1359 (2006).
[6] P. Debray, S. M. S. Rahman, J. Wan, R. S. Newrock, M. Cahay, A. T. Ngo, S. E. Ulloa, S. T. Herbert, M. Muhammad, and M. Johnson, All-electric quantum point contact spin-polarizer, Nat. Nanotechnol. **4**, 759 (2009).
[7] E. Scheer, P. Joyez, D. Esteve, C. Urbina, and M. H. Devoret, Conduction channel transmissions of atomic-size aluminum contacts, Phys. Rev. Lett. **78**, 3535 (1997).
[8] J. M. Krans, J. M. Van Ruitenbeek, V. V. Fisun, I. K. Yanson, and L. J. De Jongh, The signature of conductance quantization in metallic point contacts, Nature (London) **375**, 767 (1995).
[9] H. Overweg *et al.*, Topologically nontrivial valley states in bilayer graphene quantum point contacts, Phys. Rev. Lett. **121**, 257702 (2018).
[10] S. Goswami *et al.*, Controllable valley splitting in silicon quantum devices, Nat. Phys. **3**, 41 (2007).
[11] P. Gallagher, M. Lee, J. R. Williams, and D. Goldhaber-Gordon, Gate-tunable superconducting weak link and quantum point contact spectroscopy on a strontium titanate surface, Nat. Phys. **10**, 748 (2014).
[12] A. Jouan *et al.*, Quantized conductance in a one-dimensional ballistic oxide nanodevice, Nat. Electron. **3**, 201 (2020).
[13] J. Strunz *et al.*, Interacting topological edge channels, Nat. Phys. **16**, 83 (2020).
[14] S. Frank, P. Poncharal, Z. L. Wang, and W. A. D. Heer, Carbon nanotube quantum resistors, Science **280**, 1744 (1998).
[15] A. Yacoby, H. L. Stormer, N. S. Wingreen, L. N. Pfeiffer, K. W. Baldwin, and K. W. West, Nonuniversal conductance quantization in quantum wires, Phys. Rev. Lett. **77**, 4612 (1996).
[16] I. Van Weperen, S. R. Plissard, E. P. A. M. Bakkers, S. M. Frolov, and L. P. Kouwenhoven, Quantized conductance in an InSb nanowire, Nano Lett. **13**, 387 (2013).
[17] J. Xiang, A. Vidan, M. Tinkham, R. M. Westervelt, and C. M. Lieber, Ge/Si nanowire mesoscopic Josephson junctions, Nat. Nanotechnol. **1**, 208 (2006).
[18] C. Tan *et al.*, 2D fin field-effect transistors integrated with epitaxial high-k gate oxide, Nature (London) **616**, 66 (2023).
[19] J. Wu, Y. Liu, Z. Tan, C. Tan, J. Yin, T. Li, T. Tu, and H. Peng, Chemical patterning of high-mobility semiconducting 2D Bi_2O_2Se crystals for integrated optoelectronic devices, Adv. Mater. **29**, 1704060 (2017).
[20] T. Li and H. Peng, 2D Bi_2O_2Se: An emerging material platform for the next-generation electronic industry, Acc. Mater. Res. **2**, 842 (2021).
[21] X. Ding *et al.*, Bi_2O_2Se: A rising star for semiconductor devices, Matter **5**, 4274 (2022).
[22] J. Wu *et al.*, High electron mobility and quantum oscillations in non-encapsulated ultrathin semiconducting Bi_2O_2Se, Nat. Nanotechnol. **12**, 530 (2017).
[23] T. Li *et al.*, A native oxide high-κ gate dielectric for two-dimensional electronics, Nat. Electron. **3**, 473 (2020).
[24] Y. Zhang *et al.*, A single-crystalline native dielectric for two-dimensional semiconductors with an equivalent oxide thickness below 0.5 nm, Nat. Electron. **5**, 643 (2022).
[25] J. Tang *et al.*, Low-power 2D gate-all-around logics via epitaxial monolithic 3D integration, Nat. Mater. **24**, 519 (2025).
[26] T. Tong *et al.*, Ultrahigh Hall mobility and suppressed backward scattering in layered semiconductor Bi_2O_2Se, Appl. Phys. Lett. **113**, 072106 (2018).
[27] H. Fu, J. Wu, H. Peng, and B. Yan, Self-modulation doping effect in the high-mobility layered semiconductor Bi_2O_2Se, Phys. Rev. B **97**, 241203(R) (2018).
[28] J. Wang *et al.*, Even-integer quantum Hall effect in an oxide caused by a hidden Rashba effect, Nat. Nanotechnol. **19**, 1452 (2024).
[29] O. Zheliuk *et al.*, Quantum Hall effect in a CVD-grown oxide, Nat. Commun. **15**, 10052 (2024).
[30] R. Zhang, A. Marrazzo, M. J. Verstraete, N. Marzari, and T. D. P. Sohier, Gate control of spin-layer-locking FETs and application to monolayer LuIO, Nano Lett. **21**, 7631 (2021).
[31] Q. Liu, Y. Guo, and A. J. Freeman, Tunable Rashba effect in two-dimensional $LaOBiS_2$ films: Ultrathin candidates for spin field effect transistors, Nano Lett. **13**, 5264 (2013).
[32] J. M. Riley *et al.*, Direct observation of spin-polarized bulk bands in an inversion-symmetric semiconductor, Nat. Phys. **10**, 835 (2014).
[33] K. Wang, B. Zhang, C. Yan, L. Du, and S. Wang, Circular photocurrents in centrosymmetric semiconductors with hidden spin polarization, Nat. Commun. **15**, 9036 (2024).
[34] K. Gotlieb, C.-Y. Lin, M. Serbyn, W. Zhang, C. L. Smallwood, C. Jozwiak, H. Eisaki, Z. Hussain, A. Vishwanath, and A. Lanzara, Revealing hidden spin-momentum locking in a high-temperature cuprate superconductor, Science **362**, 1271 (2018).
[35] G. Gatti *et al.*, Hidden bulk and surface effects in the spin polarization of the nodal-line semimetal ZrSiTe, Commun. Phys. **4**, 54 (2021).
[36] Y. Cai *et al.*, Observation of highly spin-polarized dangling bond surface states in rare-earth pnictide tellurides, Adv. Mater. **37**, 2411733 (2025).
[37] E. Mikheev, I. T. Rosen, J. Kombe, F. Damanet, M. A. Kastner, and D. Goldhaber-Gordon, A clean ballistic quantum point contact in strontium titanate, Nat. Electron. **6**, 417 (2023).
[38] J. Wang, J. Wu, T. Wang, Z. Xu, J. Wu, W. Hu, Z. Ren, S. Liu, K. Behnia, and X. Lin, T-square resistivity without Umklapp scattering in dilute metallic Bi_2O_2Se, Nat. Commun. **11**, 3846 (2020).
[39] C. Tan *et al.*, Wafer-scale growth of single-crystal 2D semiconductor on perovskite oxides for high-performance transistors, Nano Lett. **19**, 2148 (2019).
[40] J. Wu, C. Tan, Z. Tan, Y. Liu, J. Yin, W. Dang, M. Wang, and H. Peng, Controlled synthesis of high-mobility atomically thin bismuth oxyselenide crystals, Nano Lett. **17**, 3021 (2017).
[41] See Supplemental Material at http://link.aps.org/supplemental/10.1103/vtjc-znrb which includes Refs. [42–67], and provides further details of the methods, calculations, and additional results of the experiment.
[42] H. J. Li, W. G. Lu, J. J. Li, X. D. Bai, and C. Z. Gu, Multichannel ballistic transport in multiwall carbon nanotubes, Phys. Rev. Lett. **95**, 086601 (2005).

[43] Y. Wang *et al.*, Ballistic PbTe nanowire devices, Nano Lett. **23**, 11137 (2023).
[44] W. Song *et al.*, Conductance quantization in PbTe nanowires, Phys. Rev. B **108**, 045426 (2023).
[45] Y. Wang *et al.*, Gate-tunable subband degeneracy in semiconductor nanowires, Proc. Natl. Acad. Sci. U.S.A. **121**, e2406884121 (2024).
[46] M. Gupta, V. Khade, C. Riggert, L. Shani, G. Menning, P. J. H. Lueb, J. Jung, R. Mélin, E. P. A. M. Bakkers, and V. S. Pribiag, Evidence for π-shifted Cooper quartets and few-mode transport in PbTe nanowire three-terminal Josephson junctions, Nano Lett. **24**, 13903 (2024).
[47] J. Gooth, M. Borg, H. Schmid, V. Schaller, S. Wirths, K. Moselund, M. Luisier, S. Karg, and H. Riel, Ballistic one-dimensional InAs nanowire cross-junction interconnects, Nano Lett. **17**, 2596 (2017).
[48] S. Heedt, W. Prost, J. Schubert, D. Grützmacher, and Th. Schäpers, Ballistic transport and exchange interaction in InAs nanowire quantum point contacts, Nano Lett. **16**, 3116 (2016).
[49] A. V. Kretinin, R. Popovitz-Biro, D. Mahalu, and H. Shtrikman, Multimode Fabry-Pérot conductance oscillations in suspended stacking-faults-free InAs nanowires, Nano Lett. **10**, 3439 (2010).
[50] A. C. Ford, S. B. Kumar, R. Kapadia, J. Guo, and A. Javey, Observation of degenerate one-dimensional sub-bands in cylindrical InAs nanowires, Nano Lett. **12**, 1340 (2012).
[51] S. Abay, D. Persson, H. Nilsson, H. Q. Xu, M. Fogelström, V. Shumeiko, and P. Delsing, Quantized conductance and its correlation to the supercurrent in a nanowire connected to superconductors, Nano Lett. **13**, 3614 (2013).
[52] J. E. Sestoft, M. Marnauza, D. Olsteins, T. Kanne, R. D. Schlosser, I.-J. Chen, K. Grove-Rasmussen, and J. Nygård, Shadowed versus etched superconductor–semiconductor junctions in Al/InAs nanowires, Nano Lett. **24**, 8394 (2024).
[53] K. Ueda *et al.*, Dominant nonlocal superconducting proximity effect due to electron-electron interaction in a ballistic double nanowire, Sci. Adv. **5**, eaaw2194 (2019).
[54] H. Zhang *et al.*, Ballistic superconductivity in semiconductor nanowires, Nat. Commun. **8**, 16025 (2017).
[55] J. Kammhuber *et al.*, Conductance quantization at zero magnetic field in InSb nanowires, Nano Lett. **16**, 3482 (2016).
[56] S. T. Gill, J. Damasco, D. Car, E. P. A. M. Bakkers, and N. Mason, Hybrid superconductor-quantum point contact devices using InSb nanowires, Appl. Phys. Lett. **109**, 233502 (2016).
[57] E. M. T. Fadaly, H. Zhang, S. Conesa-Boj, D. Car, Ö. Gül, S. R. Plissard, R. L. M. Op Het Veld, S. Kölling, L. P. Kouwenhoven, and E. P. A. M. Bakkers, Observation of conductance quantization in InSb nanowire networks, Nano Lett. **17**, 6511 (2017).
[58] J. C. Estrada Saldaña, Y.-M. Niquet, J.-P. Cleuziou, E. J. H. Lee, D. Car, S. R. Plissard, E. P. A. M. Bakkers, and S. De Franceschi, Split-channel ballistic transport in an InSb nanowire, Nano Lett. **18**, 2282 (2018).
[59] M. Sistani, P. Staudinger, J. Greil, M. Holzbauer, H. Detz, E. Bertagnolli, and A. Lugstein, Room-temperature quantum ballistic transport in monolithic ultrascaled Al–Ge–Al nanowire heterostructures, Nano Lett. **17**, 4556 (2017).
[60] D. M. Gillingham, I. Linington, and J. A. C. Bland, e^2/h quantization of the conduction in Cu nanowires, J. Phys. Condens. Matter **14**, L567 (2002).
[61] L. Olesen, E. Laegsgaard, I. Stensgaard, F. Besenbacher, J. Schiøtz, P. Stoltze, K. W. Jacobsen, and J. K. Nørskov, Quantized conductance in an atom-sized point contact, Phys. Rev. Lett. **72**, 2251 (1994).
[62] M. Brandbyge, J. Schiøtz, M. R. Sørensen, P. Stoltze, K. W. Jacobsen, J. K. Nørskov, L. Olesen, E. Laegsgaard, I. Stensgaard, and F. Besenbacher, Quantized conductance in atom-sized wires between two metals, Phys. Rev. B **52**, 8499 (1995).
[63] J. I. Pascual, J. Méndez, J. Gómez-Herrero, A. M. Baró, N. Garcia, U. Landman, W. D. Luedtke, E. N. Bogachek, and H.-P. Cheng, Properties of metallic nanowires: From conductance quantization to localization, Science **267**, 1793 (1995).
[64] Ö. Gül, D. J. van Woerkom, I. van Weperen, D. Car, S. R. Plissard, E. P. A. M. Bakkers, and L. P. Kouwenhoven, Towards high mobility InSb nanowire devices, Nanotechnology **26**, 215202 (2015).
[65] S. Krinner, D. Stadler, D. Husmann, J.-P. Brantut, and T. Esslinger, Observation of quantized conductance in neutral matter, Nature (London) **517**, 64 (2015).
[66] A. Ron and Y. Dagan, One-dimensional quantum wire formed at the boundary between two insulating $LaAlO_3/SrTiO_3$ interfaces, Phys. Rev. Lett. **112**, 136801 (2014).
[67] R. Kraft, I. V. Krainov, V. Gall, A. P. Dmitriev, R. Krupke, I. V. Gornyi, and R. Danneau, Valley subband splitting in bilayer graphene quantum point contacts, Phys. Rev. Lett. **121**, 257703 (2018).
[68] F. Wang, W. Chu, L. Huber, T. Tu, Y. Dai, J. Wang, H. Peng, J. Zhao, and X.-Y. Zhu, Phonon signatures for polaron formation in an anharmonic semiconductor, Proc. Natl. Acad. Sci. U.S.A. **119**, e2122436119 (2022).
[69] X. Zhang, Q. Liu, J.-W. Luo, A. J. Freeman, and A. Zunger, Hidden spin polarization in inversion-symmetric bulk crystals, Nat. Phys. **10**, 387 (2014).
[70] K.-F. Berggren, T. J. Thornton, D. J. Newson, and M. Pepper, Magnetic depopulation of 1D subbands in a narrow 2D electron gas in a GaAs:AlGaAs heterojunction, Phys. Rev. Lett. **57**, 1769 (1986).
[71] B. J. van Wees, L. P. Kouwenhoven, H. van Houten, C. W. J. Beenakker, J. E. Mooij, C. T. Foxon, and J. J. Harris, Quantized conductance of magnetoelectric subbands in ballistic point contacts, Phys. Rev. B **38**, 3625 (1988).
[72] I. Villar Rodriguez, Y. Gul, C. P. Dempsey, J. T. Dong, S. N. Holmes, C. J. Palmstrøm, and M. Pepper, Nonmagnetic fractional conductance in high mobility InAs quantum point contacts, Phys. Rev. B **112**, 075404 (2025).
[73] K. J. Thomas, M. Y. Simmons, J. T. Nicholls, D. R. Mace, M. Pepper, and D. A. Ritchie, Ballistic transport in one-dimensional constrictions formed in deep two-dimensional electron gases, Appl. Phys. Lett. **67**, 109 (1995).

[74] W. P. Su, J. R. Schrieffer, and A. J. Heeger, Solitons in polyacetylene, Phys. Rev. Lett. **42**, 1698 (1979).
[75] D. Kaplan, A. Stern, and B. Yan, Even integer quantum Hall effect in materials with hidden spin texture, arXiv:2406.03448.
[76] E. Prada, P. San-Jose, M. W. A. De Moor, A. Geresdi, E. J. H. Lee, J. Klinovaja, D. Loss, J. Nygård, R. Aguado, and L. P. Kouwenhoven, From Andreev to Majorana bound states in hybrid superconductor–semiconductor nanowires, Nat. Rev. Phys. **2**, 575 (2020).
[77] J. Xiao, Data for Quantized conductance in a CVD-grown nanoribbon with hidden Rashba effect, Zenodo, 10.5281/zenodo.18050797 (2025).